

Mixing of the Immiscible Liquids in the Entrance Region of a T-Type Chamber Using Laser Induced Fluorescence (LIF) Method

A. A. Sarbanha, F. Sobhanian, S. Movahedirad*

School of Chemical Engineering, Iran University of Science and Technology (IUST), I.R.Iran

ARTICLE INFO

Article history:

Received: 2015-11-10

Accepted: 2016-03-03

Keywords:

Laser Induced Fluorescence
(LIF)

T-Type Chamber

Liquid Mixing

Mixing Index

ABSTRACT

A Laser Induced Fluorescence technique (LIF) has been used to study the mixing behavior of two emerging streams in a T-Type mixing chamber. A mixing index on the basis of digital image light intensities is calculated. It has been shown that averaging over more than 800 images leads to a stable mixing index calculation. Moreover, the effect of equal and un-equal flow rates on the mixing behavior of the streams has been studied. The results show that the histograms of the light intensity changes from double peak (unmixed) to a single peak (mixed) at high elevations of the chamber. Mixing index has a linear descending behavior moving toward the cell front wall and it was shown that the mixing index can be reduced up to 50% moving from cell center to near wall region. Moreover, there is a transition zone in both equal and un-equal fluid flow rates in mixing index. It was shown that the third component velocity plays an important role in mixing behavior in T-Type mixing chamber.

1. Introduction

The term 'mixing' is applied to the processes used to reduce the degree of non-uniformity or gradient of a property such as concentration, viscosity, temperature in a system in order to achieve a desired degree of homogeneity at various length scales [1]. Mixing is also important in advancing both heat and mass transfer in reactors. The quality of mixing of materials greatly determines the success and efficiency of many industrial processes, while ineffective mixing results in considerable economic and environmental implications [2]. There is some evidence that bad mixing of species in reactors leads to a long reaction time [3].

Mixing processes of liquid-liquid components are of great technical interest in many industries, mainly in chemical industries. Besides the numerous technical researches in this field, the mixing processes are not completely predictable. The mixing phenomenon is actually characterized by observation rather than by basic knowledge. Local mixing quality is a crucial parameter influencing the economics of such processes [4].

In batch reactors, mixing is a transient process that occurs over time, thus the concentration of materials in all space directions changes with time. On the other

*Corresponding author: movahedirad@iust.ac.ir

hand, a continuous process usually has a main transfer direction, the axial direction. Although mixing in the axial direction is not desirable because it reduces the conversion and selectivity. Consequently, the mixing should be ideal anisotropic. Since this condition cannot be fully achieved, the secondary flow can be used to experience this behavior approximately. In geometry similar to duct, this issue led to T-type reactor or zigzag canals with T-type entrance [3].

This configuration usually consists of two opposing feeding pipes or ducts opening in a main duct under different angles, leading to two impinging jets in a confined space [5]. Efficiency of the mixing in such a device is determined by the characteristics of the flow, e.g. the Reynolds number, the inflow conditions and the mixer geometry [5]. By changing these process parameters the product properties might be adjusted to the desired values.

Several authors have used flow visualization techniques with passive tracers to study mixing in these mixers [6]. The main concern has been the study of the mixing mechanisms in opposing jets and evaluation of the effect of operational conditions or geometrical parameters on mixing quality [6].

Lee *et al.* [7] have taken high speed photographs of the flow in a transparent Plexiglas mixing chamber. Tucker and Suh [8] used an ink tracer to detect flow structures in the impinging jets flow, quantifying the mixing quality from the variance of the photographed concentration fields. Technological limitations at that time and the rapid motion of the formed vortices hindered the clear visualization of the flow from both methods of Lee *et al.* [7], and Tucker III and Suh [8], for $Re > 150$. To overcome this limitation, Sandell *et al.* [9], adopted a more

advanced technique with thymol blue, a indicator used as a dye that fades with mixing. Thymol blue in stagnant tap water takes about half an hour to fade, but rapidly fades with agitation. Wood *et al.* [10], captured images of mixing reactors flow seeded with polystyrene particles with an average diameter of 100 μm . The shutter speeds on the camera were varied so that the particles present in the fluid appeared as streaks in the images. More recently, flow laser induced fluorescence visualization techniques, μ -LIF by Hoffmann *et al.* [11], and PLIF by Sultan *et al.* [12], have also been used to study different flow regimes and mixing quality in impingement mixing in micro mixers with rectangular cross-sections.

Laser-induced fluorescence (LIF) is a non-intrusive technique for measuring scalar concentrations in fluid flows [14]. The most common application of LIF in fluid flows is two-dimensional planar laser induced fluorescence (PLIF). [14] In PLIF, a laser is used to excite a fluorescent species within the flow. Typically, the tracer is an organic fluorescent dye such as fluorescein or rhodamine. The dye absorbs a portion of the excitation energy and spontaneously re-emits a portion of the absorbed energy as fluorescence. The fluorescence is measured optically and used to infer the local concentration of the dye.

In the present work, the PLIF technique is used for the visualization and study of the mixing index in a small scale T-type mixing chamber. The effect of flow imbalance on the obtained mixing quality is also studied by changing the inlet volumetric flow rate ratio.

2. Experimental

2.1. Experimental setup and equipment

A Schematic of the experimental set-up is

shown in Fig. 1. Pure water enters the chamber from one side and the stream contains Rhodamine-B enters from another side. The flow rates are measured before entering the chamber using two rotameters. The camera is installed near the chamber perpendicular to the laser sheet according to Fig. 1.

The optical arrangement for fluorescence detection is shown in Fig. 2. The light source was a diode laser with maximum 0.880 W energy level and 532 nm wavelength. Laser sheet was formed by a rotating polygon with mirrors on each face. This polygon is rapidly rotated such that each face produces a single laser scan. The light sheet crosses the cell walls at different sides and depth of the

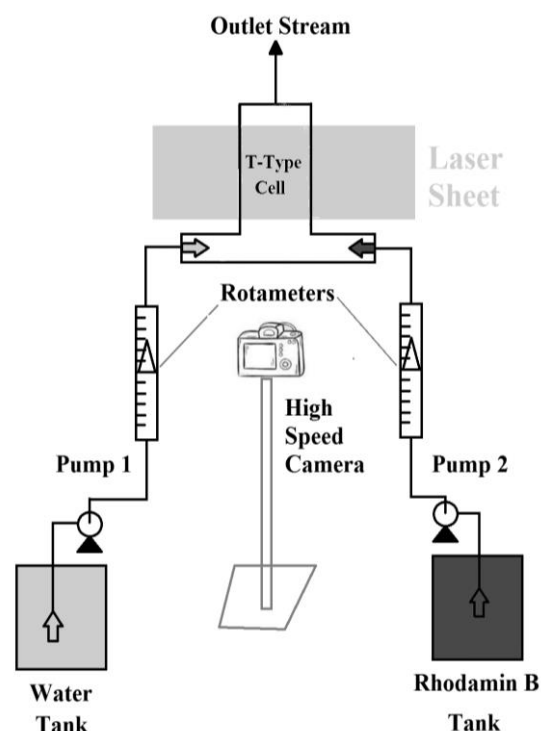


Figure 1. –A schematics of the experimental set-up.

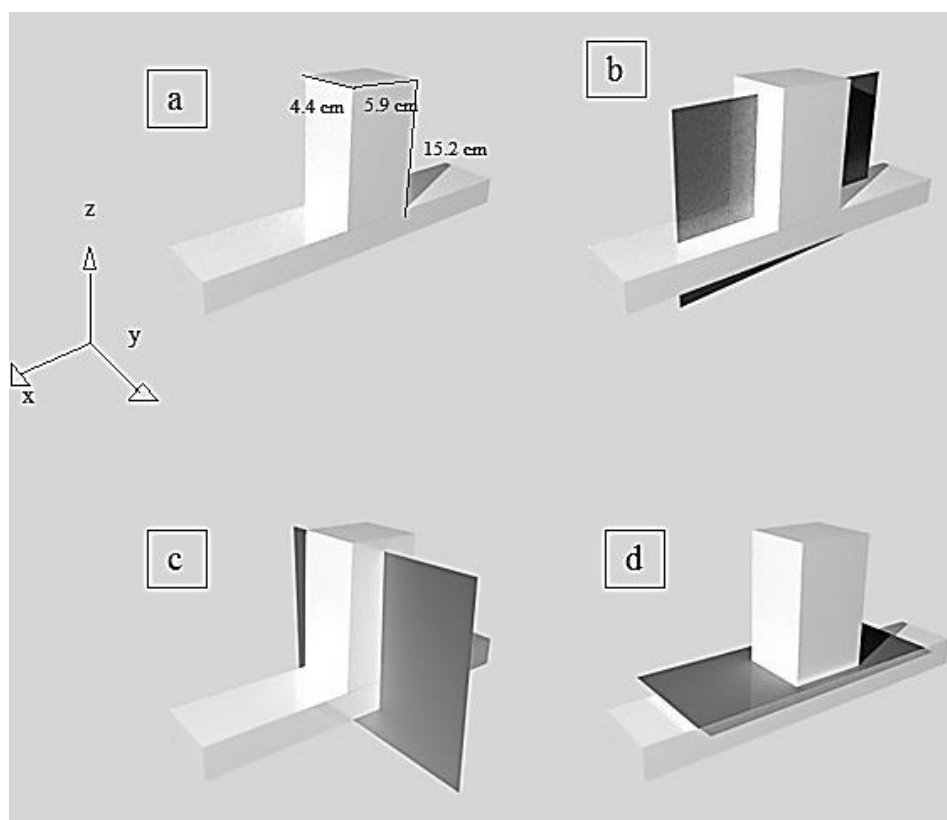


Figure 2. a) The cell schematics with internal dimensions and b) front view, c) lateral view and d) cross sectional view of the cell (green sheet is the laser sheet).

column. A CMOS camera (CASIO EX-ZR700) placed perpendicular to the laser sheet was used to capture instantaneous images with 4608×3456 pixels. Other camera specifications are given in Table 1. For LIF analysis purpose, a filter was placed in front of the camera lens to block the scattered laser light but to pass the fluoresced wavelength. The images were captured in three dimensions of front side, lateral side and cross sectional side as can be seen in Fig. 2.

2.2. Materials and methods

General factors that influence on the dye selection are the compatibility of the selected dye with excitation laser, large separation between absorption and emission peaks and high quantum efficiency [14]. Rhodamine B (Merck/casting number:536092) was chosen as a fluorescent dye, because its peak absorption is at 555 nm which is very close to the emitted wavelength of the incident diode laser. Rhodamine B absorption spectrum is broad enough to permit excitation at either 514.5 or 532 nm.

3. LIF theory

Laser Induced fluorescence (LIF) is one of the quantitative flow visualization methods that can be used to measure the scalar quantities such as temperature and concentration [13]. Temporal concentration of a fluorescent dye can be measured in a

Table 1.

Camera specifications.

Image dimension (pixel)	4608×3456
Pixel number (MP)	16.1
Sensor type	CMOS
Optical zoom	16X

flow chamber to obtain more insight about the mixing behaviour of the fluid streams.

The theory of the LIF is on the basis of the filtering of emitted light of a fluorescent dye mixed in the fluid from illuminating light of a laser source. The light emitted from the fluorescent dye has a greater wavelength than the laser excitation light (see Fig. 3)

According to the Beer–Lambert law [13], the light intensity decay due to dye absorption can be expressed as: [14]

$$\frac{dI}{I} = -\epsilon C dr \quad (1)$$

Where I is the light intensity, dr is the distance the light travels in the medium, C is the dye concentration and ϵ is the absorption coefficient [13].

In planar laser induced fluorescence (PLIF) applications, at radial distances that are large compared to the incoming beam diameter, the sheet will have an intensity distribution of the general form

$$I(r, \theta, z) = Pa(r, \theta)f(r)g(\theta)h(z) \quad (2)$$

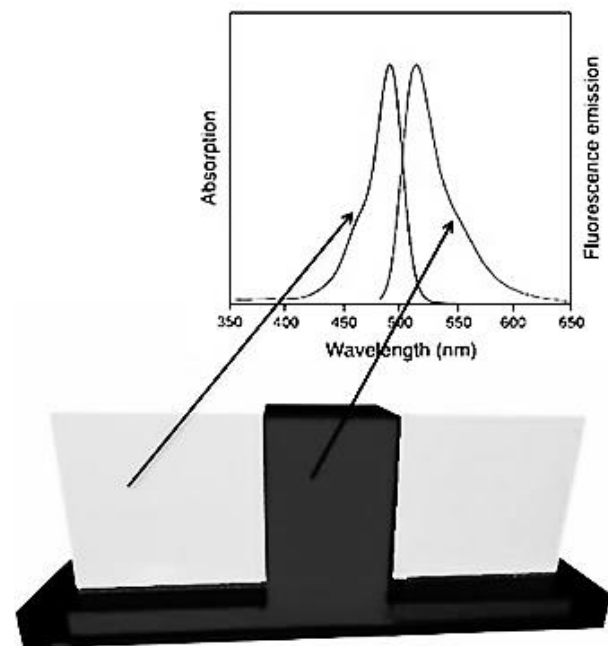


Figure 3. Schematics that show the concept behind LIF theory.

where P is the power of the incoming beam, $f(r)g(h)h(z)$ is attenuated spatial intensity distribution of the sheet and as a result of Beer-Lambert's law $a(r, \theta)$ is the dimensionless attenuation along ray paths due to dye absorption according to Crimaldi [14]:

$$a(r, \theta) = \exp\left[-\epsilon \int_0^r C(r', \theta) dr'\right] \quad (3)$$

Where, r and θ are the radial distance from the Laser origin, and cylindrical coordinate parameter that shows the laser beam passage to make a sheet, respectively.

The fluorescence intensity sensed by a CCD camera at pixel location (i, j) is thus:

$$I_F(i, j) = \beta(i, j) \frac{F}{\Delta A} = \alpha(i, j) a(r, \theta) C \quad (4)$$

Where ΔA is the target area, F is the local fluorescence, $\beta(i, j)$ is the fraction of the total omni-directional fluorescence received by the camera optics at a particular pixel location, and $\alpha(i, j)$ is the collection of concentration independent constants [14].

$$\alpha(i, j) = \beta(i, j) \phi \epsilon P f(r) g(\theta) \quad (5)$$

Raw PLIF images captured by the camera need to be post processed for error correction and calibration.

When more fluorescent dyes in addition to the background are present, the recorded fluorescence intensity in the n^{th} image is:

$$I_n(i, j) = \alpha(i, j) a_c(r, \theta) a_b(r) [c_n(i, j) + b_n] + D(i, j) \quad (6)$$

where $D(i, j)$ is the dark-response of the camera. The dark response can be quantified as the average light intensity of a number of images acquired with the lens cap covered. The dye concentrations present in the n^{th} image are decomposed as: $C_n(i, j) = c_n(i, j) + b_n$, where b_n is the uniform background concentration present at the time

the image was taken, and $a(r, \theta) = a_c(r, \theta) a_b(r)$, where a_c and a_b are the local attenuations due to c_n and b_n , respectively. [14].

The fluorescence intensity related to the uniform background is:

$$B_n(i, j) = \alpha(i, j) a_b(r) b_n + D(i, j) \quad (7)$$

$I_n(i, j)$ and $B_n(i, j)$ can be combined to give a term for $C_n(i, j)$ that does not include any definite reference to $\alpha(i, j)$: [14]

$$c_n(i, j) = \frac{b_n}{a_c(r, \theta)} \frac{I_n(i, j) - [a_c(r)(B_n(i, j) - D(i, j)) + D(i, j)]}{B_n(i, j) - D(i, j)} \quad (8)$$

For more details of the PLIF theory, interested reader can refer to Crimaldi [14].

4. Results and discussion

4.1. Digital image processing

The mixing process is a random phenomenon, so statistical analysis is an important tool for studying this process. In statistics the standard deviation is a measure that indicates how data is spread around the mean value.

Standard deviation for a two-component mixture is calculated as follows:

$$\delta = \sqrt{\sum_{i=1}^2 \frac{(X_i - \bar{X})^2}{2 - 1}} \quad (9)$$

Figs. 4a and 4b show the cross sectional area images at different distances from cell bottom, respectively. The light intensity histograms of these figures are shown in Figs. 4c and 4d. As can be seen from these figures by increasing the distance from the cell bottom, mixing phenomena becomes better so data dispersion became less and histograms became more uniform.

Consider a two-component mixture containing mole fraction x_A of component A

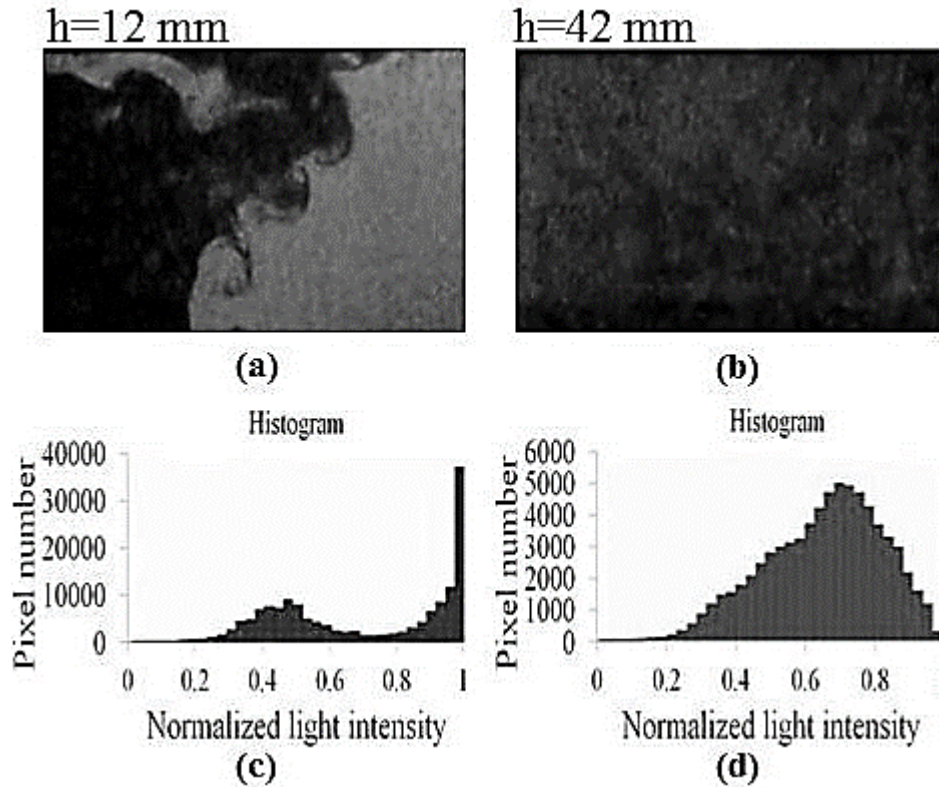


Figure 4. Increasing the mixing and better histogram with increasing the distance from the cell bottom.

and mole fraction x_B of component B . Without mixing, both components are pure. By multiple sampling of mixture, it is expected that the percentage of samples containing A is x_A so the deviation of this component rather than pure component is $(1-x_A)$. Similarly, the percentage of the sample that has pure B is x_B . In this case, the deviation of the component B at the pure component A is $(0-x_A)$. By combining these two expressions in terms of mole fraction x_A and according to the fact that $x_A+x_B=1.0$:

$$\begin{aligned} \delta_0^2 &= 1/N [x_A N(1-x_A)^2 + (1-x_A)N(0-x_A)^2] \\ &= x_A(1-x_A) \end{aligned} \quad (10)$$

For a two-component mixture average mole fraction is calculated as follows [14]:

$$\bar{X} = \frac{1}{2} \sum_{i=1}^{i=2} X_i \quad (11)$$

Where i is the number of each component,

and X is the mole fraction of each component.

Rose proposed the following expression for mixing index evaluation [15]:

$$M = 1 - \frac{\delta}{\delta_0} \quad (12)$$

In the case of non-mixing, the mixing index M becomes zero. For the fully mixed state, the mixing index should be unity. Different equations have been used for calculating mixing index in literature [15]. Table 2 shows a list of different mixing indices which have been used for characterization of liquids mixing. In the present work Eq. 13 has been used to study the mixing behavior of two liquid streams. The light intensity value for each pixel varying from 0 to 255 is read at the selected region and the mixing index I_E is calculated as follows: [17]

$$I_E = 1 - \frac{1}{\bar{I}} \sqrt{\frac{1}{N} \sum (I_i - \bar{I})^2} \quad (13)$$

Table 2.

List of different mixing indices that have been used for characterization of liquids mixing.

Ref.	Mixing index	explanation
P. Lacey (1954) [16]	$I_M = (\sigma_0^2 - \sigma^2)/(\sigma_0^2 - \sigma_r^2)$	σ standard deviation σ_0 maximum deviation σ_r random standard deviation $I_M=1$ fully mixed $I_M=0$ non-mixing
Rose <i>et al.</i> (1959)[15]	$M = 1 - \frac{\delta}{\delta_0}$	δ standard deviation δ_0 maximum deviation $M=1$ fully mixed $M=0$ non-mixing
D. W. Oh <i>et al.</i> (2007)[17]	$I_E = 1 - \frac{1}{\bar{I}} \sqrt{\frac{1}{N} \sum (I_i - \bar{I})^2}$	\bar{I} averaged light intensity of the region $\bar{I} = \sum I_i/N$ N total number of pixels I_i value of light intensity at each single pixel $I_E=1$ fully mixed $I_E=0$ non-mixing
C. T. Wang <i>et al.</i> (2010) [18]	$\varepsilon_{mixing} = 1 - \frac{1}{L} \int_0^L \left \frac{X_{A,outlet} - 0.5}{X_{A,max} - 0.5} \right dx$	$X_{A,outlet}$ maximum mole fraction of fluid A $X_{A,max}$ mole fraction of fluid A in outlet L channel outlet wide $\varepsilon_{mixing}=1$ fully mixed $\varepsilon_{mixing}=0$ non-mixing
T. N. Le <i>et al.</i> (2010) [19]	$I = \frac{1}{\bar{C}} \sqrt{\frac{1}{N} \sum_i^N (C_i - \bar{C})^2}$	\bar{C} average concentration of the region N total number of pixels C_i value of light intensity at each single pixel $I=1$ fully mixed $I=0$ non-mixing

Where \bar{I} is the averaged light intensity of the region which is defined as $\bar{I} = \sum I_i/N$, N denoting the total number of pixels in the region, and I_i is the value of light intensity at each single pixel [14].

4.2. Averaging over images

To have a reliable judgment about the mixing behaviour it is important to show that the results of MI at every fluid flow rate are averaged over adequate number of images. In this regard, first a sufficient number of images for averaging should be evaluated. Fig. 5 shows that average value of MI over 800 images and more converge to a constant

value. In other words, using more than 800 images for averaging produces a reasonable and authentic result. In this article 1000 images were used for averaging to confirm that results are authentic.

4.3. Effect of distance from front wall

It is important to know more about the mixing behavior of the streams at different layers from cell wall. The wall effects could be studied easily by moving laser sheet toward the front wall.

Fig. 6 shows that mixing index increases by taking distance from the front wall. As can be seen from this figure the mixing index

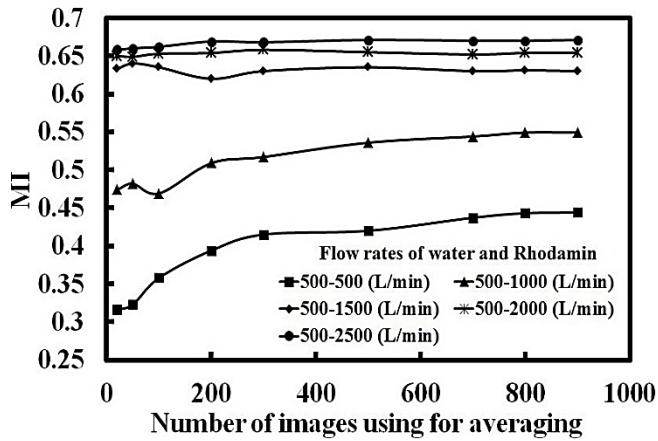


Figure 5. Effect of number of images used for averaging in mixing index at five different flow rates.

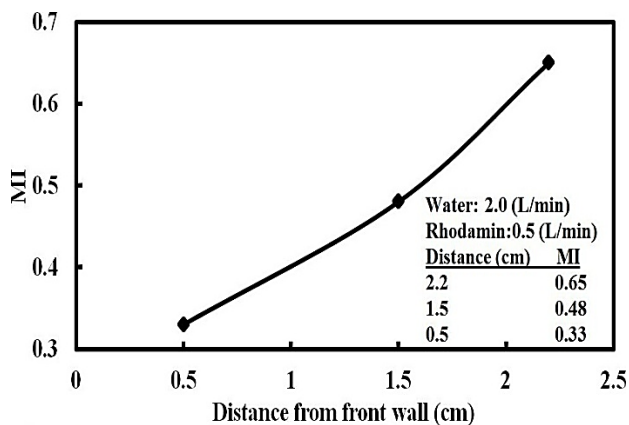


Figure 6. Effect of distance of illuminating sheet from front wall.

at the center sheet is the maximum value and there is an approximately linear decreasing pattern for MI toward the chamber wall. As can be observed from this Figure the MI decreases up to 50%, moving from cell center to the near wall region.

In the following sections the mixing index at the central sheet (distance from wall=2.2 cm) are reported.

4.4. Effect of liquid flow rates at equal quantities

As expected, Fig. 7 shows that increasing flow rates in equal quantities results in increasing the mixing indices. As can be seen from this Figure, an S-shape curve is seen by plotting MI versus total flow rate. There is a transition zone between the total

flow rates of 2 and 3 L/min which can be attributed to the 3-Dimensional effect of flow that is described in more detail in section 4-5. Before and after this transition zone the MI remains almost constant.

4.5. Effect of imbalance in liquid flow rates

Fig. 8 shows the variations of MI versus total flow rates of streams at imbalance flow rates. The water flow rate is constant and the flow rate of the stream containing Rhodamine B is variable. As can be observed from this Figure the MI increases until it reaches a constant value. In the present case, by increasing the flow rate of Rodamin contained stream one side flow is dominant and consequently the color of that stream becomes dominant, at least at the entrance zone. At higher elevations the mixing develops and helps to obtain a better MI. The

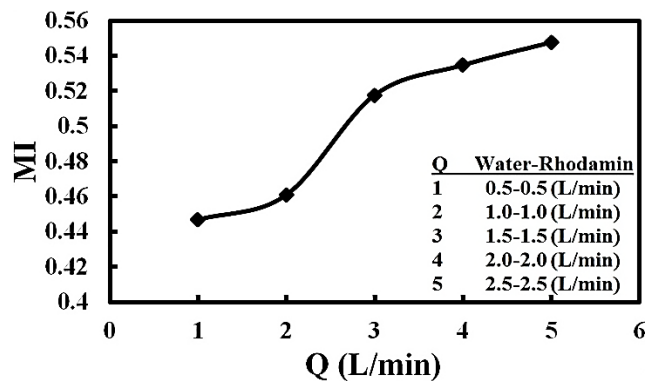


Figure 7. Effect of increasing liquids flow rates in equal quantities on the mixing index.

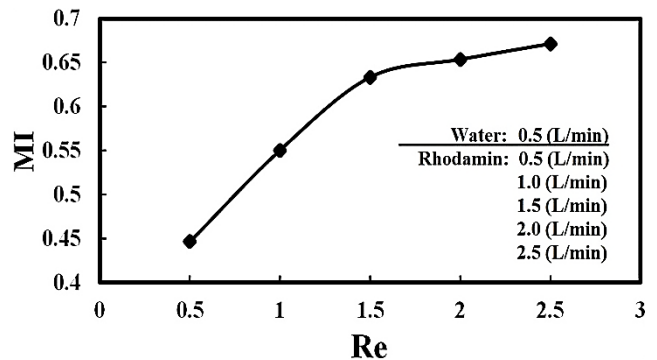


Figure 8. MI versus total flow rates at imbalance flows of two streams.

average MI shows after total flowrate of 2 L/min the MI remains approximately constant.

As it was noted in section 4-4 the third component of velocity improves the mixing of two streams. To show this concept the particle image velocity (PIV) technique is used at the cross sectional area of the cell (see Fig. 9). The averaged velocity field of the flow at $h=2.0$ cm shows that by increasing the right hand side flow rate the vortex loop develops and fills the total cross section of the cell. Obviously this third component velocity enhances the mixing of two streams.

5. Conclusions

PLIF technique has been used to study the mixing of two impinging streams in a T-shape mixing chamber. Briefly the following results have been obtained in this experimental work:

- The histograms of the light intensity of the imaged captured with the filter changes from a double peak (unmixed) to a more uniform single peak (mixed) pattern going far from the cell bottom.
- The experimental data show that averaging MI over at least 800 images leads to a reasonable and authentic result.
- Going toward the cell front wall shows that the mixing index decreases linearly and changes from about 0.68 at the cell center to approximately 0.33 at the adjacent front wall at total flow rate of $Q=2.5$ L/min . This is due to the wall damping effect.
- At equal flow rate conditions there is a transition zone between total flow rates of 2 and 3 L/min., after that the mixing index flattened.
- The imbalance in two flow streams has been studied in this paper and in both equal

and un-equal fluid flow rates it was shown that the third component of flow velocity can lead to a vortex formation in the cross sectional area of the chamber and can influence on the mixing index.

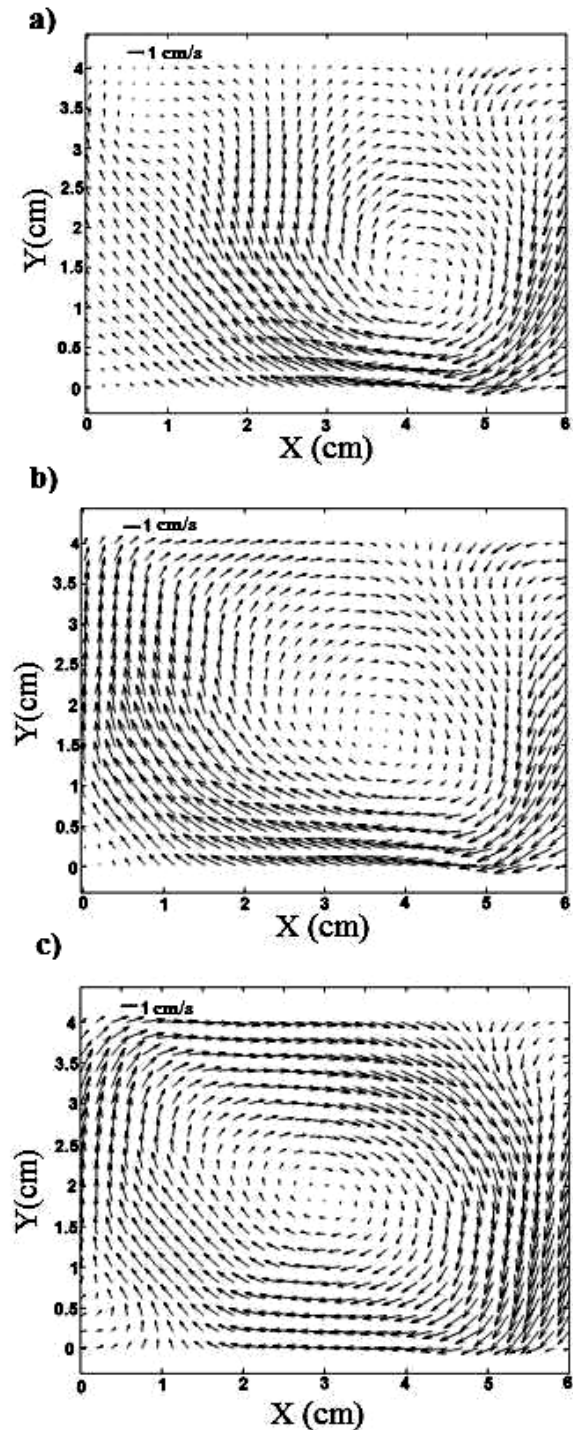


Figure 9. Averaged PIV results of the flow at the cross sectional view of the cell at $h=2.0$ cm , right hand side stream flow rates: a) 0.5, b)1.5 and c) 2.0 L/min.

Abbreviations

LIF	Laser Induced Fluorescence
PLIF	Planar Laser Induced Fluorescence
CMOS	Complementary Metal-Oxide Semiconductor
CCD	Charge-coupled Device
MI	Mixing Index

References

- [1] Chhabra, R. P. and Richardson, J. F., *Non-Newtonian Flow and Applied Rheology*, 2nd ed., Elsevier, p. 376 (2011).
- [2] Boodhoo, K. V. K. and Al-Hengari, S., "Micromixing characteristics in a small scale spinning disc reactor", *Chem. Eng. Tech.*, **35** (7), 1229 (2012).
- [3] Suh, Y. K. and Kang, S., "A Review on Mixing in Microfluidics" *Micromachines*, **1**, 82 (2010).
- [4] Bockhorn, H. Mewes, D. Peukert, W. and Warnecke, W. H. J., *Micro and Macro Mixing: Analysis, Simulation and Numerical Calculation*, 1st ed., p. 69 (2009).
- [5] Schwertfirm, F. Gradl, J. Schwarzer, H. C. and Manhart, P. M. "The low Reynolds number turbulent flow and mixing in a confined impinging jet reactor", *Int. J. Heat Fluid Flow*, **28**, 1429 (2007).
- [6] Fonte, C. P. Sultan, M. A. Santos, R. J. Dias, M. M. and Lopes, J. C. B. "Flow imbalance and Reynolds number impact on mixing in Confined Impinging Jets", *Chem. Eng. J.*, **260**, 316 (2015).
- [7] Lee, L. J. Ottino, J. M. Ranz, W. E. and Macosko, C. W. "Impingement mixing in reaction injection molding", *Polymer Eng. Sci.*, **20**, 868 (1980).
- [8] Tucker, C. L. and Suh, N. P. "Mixing for reaction injection molding Impingement mixing of liquids", *Polymer. Eng. Sci.*, **20**, 875 (1980).
- [9] Sandell, D. J. Macosko, C. W. and Ranz, W. E. "Visualization technique for studying impingement mixing at representative Reynolds numbers", *Polymer. Proc. Eng.*, **3**, 57 (1985).
- [10] Wood, P. Hrymak, A. Yeo, R. and Johnson, D. Tyagi, A., "Experimental and computational studies of the fluid mechanics in an opposed jet mixing head", *Phys. Fluids*, 1362 (1991).
- [11] Hoffmann, M. Schluter, M. and Rabiger, N. "Experimental investigation of liquidliquid mixing in T-shaped micro-mixers using I-LIF and I-PIV," *Chem. Eng. Sci.*, **61**, 2968 (2006).
- [12] Sultan, M. A. Fonte, C. P. Dias, M. M. Lopes, J. C. B. and Santos, R. J. "Experimental study of flow regime and mixing in T-jets mixers", *Chem. Eng. Sci.*, **73**, 388 (2012).
- [13] Walker, D. A., "A fluorescence technique for measurement of concentration in mixing liquids", *J. Phys. Sci. Instru.*, **20**, (1987).
- [14] Crimaldi, J. P. "Planar laser induced fluorescence in aqueous flows", *Exp. Fluids*, **44**, 851 (2008).
- [15] Rose, H. E., "A suggested equation related to the mixing of powders", *Trans. Inst. Chem. Eng.*, **37**, 47 (1959).
- [16] Lacey, P. "Developments in theory of particulate mixing", *J. Appl. Chem.*, **4**, 257 (1954).
- [17] Oh, D. W. Jin, J. S. Choi, J. H. Kim, H. Y. and Lee, J. S. "A microfluidic chaotic mixer using ferrofluid, iop publishing, *J. micromech. microeng.*, **17**, 2077 (2007).
- [18] Wang, C. T. and Hu, Y. C. "Mixing of Liquids Using Obstacles in Y-Type Microchannels", *Tamkang Jour. of Sci. Eng.*, **13** (4), 385 (2010).

- [19] Le, T. N. Suh, Y. K. and Kang, S. "A numerical study on the flow and mixing in a microchannel using magnetic particles", *J. Mech. Sci. Tech.*, **24**, 441(2010).